

Deep Unfolding with Normalizing Flow Priors for Inverse Problems

Xinyi Wei¹, Hans van Gorp¹, Lizeth Gonzalez Carabarin¹, Daniel Freedman², Yonina Eldar³, and Ruud van Sloun^{1,4}

¹*Eindhoven University of Technology*

²*Google Research*

³*Department of Math and Computer Science, Weizmann Institute of Science, Rehovot, Israel*

⁴*Philips Research, Eindhoven, The Netherlands*

Abstract—Many application domains, spanning from computational photography to medical imaging, require recovery of high-fidelity images from noisy, incomplete or partial/compressed measurements. State of the art methods for solving these inverse problems combine deep learning with iterative model-based solvers, a concept known as deep algorithm unfolding. By combining a-priori knowledge of the forward measurement model with learned (proximal) mappings based on deep networks, these methods yield solutions that are both physically feasible (data-consistent) and perceptually plausible. However, current proximal mappings only implicitly learn such image priors. In this paper, we propose to make these image priors fully explicit by embedding deep generative models in the form of normalizing flows within the unfolded proximal gradient algorithm. We demonstrate that the proposed method outperforms competitive baselines on various image recovery tasks, spanning from image denoising to inpainting and deblurring.

Index Terms—Deep unfolding, normalizing flow, inverse problem, image reconstruction

I. INTRODUCTION

IMAGE reconstruction from noisy, partial or limited-bandwidth measurements is an important problem with applications spanning from fast Magnetic Resonance Imaging (MRI)[1] to photography [2]. These reconstruction tasks can be posed as linear inverse problems, which are however often ill-posed, with many potential solutions satisfying the measurements. Recovery of a meaningful and plausible solution thus requires adequate statistical priors. Formulating such priors for natural or medical image recovery is however not trivial and likely dependent on the recovery task itself. Traditional convex optimization methods for, e.g., compressed sensing assume sparsity in some transformed domain [3], [4]. Choosing an appropriate sparse basis is however highly dependent on the application and requires careful analysis of, e.g., wavelet or total variation-based regularizers that are in practice hard to tune. Later, so called plug-and-play methods started to adopt pretrained deep-learning-based denoisers into proximal-gradient optimization algorithms. Generative neural models, such as generative adversarial networks (GANs) [5] and normalizing flows [6], allow for explicit modelling of the priors and have also been adopted within iterative optimization frameworks. While all of these approaches improve upon the hand-crafted sparsity-based priors and exhibited great empirical success, they

do not accelerate the optimization process and still rely on time-consuming iterative algorithms. Moreover, their strength, being agnostic of the task and merely concerned with modeling the general image prior, is also a limitation: these approaches do not exploit task-specific statistical properties that can aid the optimization.

Deep algorithm unfolding aims to address these problems by unrolling the iterative optimization algorithm as a feed forward deep neural network [7], [8]. The result is a deep network that takes the structure of the iterations in proximal-gradient methods, but allows for learning the successive “neural” proximal mappings directly from training data [9]. Deep algorithm unfolding has greatly accelerated compressive imaging, requiring far less folds/iterations than its conventional counterparts by fully adapting and tuning the optimization algorithm to the specific domain/data and task through learning.

However, these fast and task-based neural unrolled proximal gradient descent methods no longer explicitly model the underlying statistical priors as a data-generating probability density function. Instead, current methods rely on “discriminative” network architectures to model the proximal mapping, such as Resnet- or U-net-based architectures. Despite their success and vast application space, such implicit priors via neural mappings complicate analysis and steer away from a probabilistic interpretation and modeling of the data distribution.

In this paper, we propose an end-to-end deep algorithm unfolding framework that combines neural proximal gradient descent with generative normalizing flow priors. Our approach first pre-trains a generic flow-based model on natural images by direct likelihood maximization, and subsequently fine-tunes the entire pipeline and priors to adapt to specific image reconstruction tasks.

Our main contributions are:

- We propose a new framework for solving linear inverse problems based on deep algorithm unfolding and normalizing flow priors that adapt to the data and task.
- We leverage the generative probabilistic nature of our model to yield a strong initial guess: the maximum likelihood solution of the learned flow prior.
- We demonstrate strong performance gains over state-of-the-art neural proximal gradient descent baselines on a wide range of image restoration problems.

II. RELATED WORK

A. Deep learning for image reconstruction

Deep learning [10] is increasingly adopted for image reconstruction tasks, outperforming traditional iterative-based reconstruction methods for tasks such as image denoising [11], [12], [13], [14], [15], deconvolution [16], inpainting [17] [18] and end-to-end signal recovery [19] [20] [21][22]. More specifically, within the framework of compressed sensing, in which signals are to be reconstructed from a set of compressed measurements, deep learning methods have improved both image quality and reconstruction speed [23], [24].

B. Optimization using deep denoisers and generative models

Recent works have shown that, using variable splitting techniques [25], [26], any preferred denoiser can be used within (plugged into) classical model-based optimization methods (so called “plug-and-play” approaches). Typical denoising architectures include are based on convolutional autoencoders, U-Nets [27], or ResNets [28]. An interesting special case to note is DRUNet, having the ability to handle various noise levels via a single model [29]. Related to this, Deep generative models (DGMs), such as generative adversarial networks (GANs) [30], variational autoencoders (VAEs) [31] and normalizing flows [32], can also serve as meaningful priors for inverse problems in imaging [33], [34], [24], [35], [6]. DGMs generate a complex distribution (e.g. that of natural images) from a simple latent base distribution (e.g. independent Gaussians) using a learned deterministic transformation, obtained by pretraining on a large dataset of clean images. This pretrained model is subsequently used to solve inverse problems by performing gradient-based optimization in their (possibly lower dimensional) latent space.

While optimization algorithms that make use of deep denoisers and generative models have shown strong empirical performance, their time-consuming iterative nature makes them slow. Moreover, these approaches do not exploit task-specific information to aid the optimization process.

C. Deep algorithm unfolding

In deep (algorithm) unfolding, the structure of model-based iterative optimization algorithms is unfolded/unrolled into a fixed-length feedforward neural network [7], [8]. The parameters of the unfolded algorithm are then trained using deep-learning approaches [36]. Examples include ADMM-Net, an unfolded version of the iterative ADMM solver [37], and ISTA-Net, integrating convolutional networks with sparse-coding-based soft thresholding activations [38]. Other works include D-AMP [39] [40] inspired by the approximate message passing (AMP) algorithm, neural proximal gradient descent [9], and approaches that unfold primal-dual solvers [41][42] or half-quadratic splitting methods [43][44].

Unlike current deep algorithm unfolding methods, which rely on non-generative neural models to learn their proximal mappings, we here propose to integrate deep generative (normalizing flow) models into their unrolled architectures. This results in an interpretable deep network that explicitly models the image prior and adapts it to its task by end-to-end training.

III. PROBLEM FORMULATION

We concern consider problems of the following form:

$$y = \mathbf{A}x + \eta, \quad (1)$$

where $y \in \mathbb{R}^m$ is a noisy measurement vector, $x \in \mathbb{R}^n$ is the desired signal/image expressed in vector form, $\eta \in \mathbb{R}^m$ is a noise vector, and $\mathbf{A} \in \mathbb{R}^{m \times n}$ is a measurement matrix, which we here assume to be known. For the ill-posed inverse problems that we are interested in, maximum-likelihood estimation, i.e., $\arg\max_x p(y|x)$, is insufficient, yielding solutions that adhere to the measurement model but are visually implausible. By imposing statistical priors, meaningful solutions (i.e. those that fit expected behavior and prior knowledge) can be obtained through maximum a posteriori (MAP) inference:

$$\hat{x}_{MAP} := \arg\max_x p(x|y) \propto \arg\max_x p(y|x) p_\theta(x), \quad (2)$$

where $p(y|x)$ is the likelihood according to the linear noisy measurement model, and $p_\theta(x)$ is the signal prior. The effectiveness of MAP inference strongly depends on the adequacy of the chosen prior. Formalizing such knowledge is challenging and requires careful analysis for each domain (e.g., natural images vs medical images) and recovery task (e.g., denoising vs inpainting). Assuming a Gaussian distribution of measurement model errors, i.e. $p(y|x) \sim \mathcal{N}(\mu = \mathbf{A}x, \sigma_n^2)$, MAP optimization leads to the following (negative log posterior) minimization problem:

$$\hat{x} = \arg\min_x \frac{1}{2\sigma_n^2} \|y - \mathbf{A}x\|_2^2 - \log p_\theta(x). \quad (3)$$

Given (3), our goal is now twofold: 1) to learn a useful prior $p_\theta(x)$, and 2) to accelerate standard gradient-based optimization of (3) using deep algorithm unfolding. We will address the former in the next section, and then proceed with the latter in section IV-B.

IV. DEEP ALGORITHM UNFOLDING WITH FLOW PRIORS

In section we present the framework of the proposed architecture.

A. Flow priors

Normalizing flows [32] are a class of generative models, which are capable of modeling powerful and expressive priors for natural images. Normalizing flows transform a base probability distribution $p(z) \sim \mathcal{N}(0, I)$ into a more complex, possibly multi-modal distribution by a series of composable, bijective, and differentiable mappings.

Due to the invertible nature of normalizing flow models, they can operate in both directions. These are the generative direction, which generates an image from a point in latent space ($x = g_\theta(z)$), and the flow direction, which maps images into its latent representation ($z = f_\theta(x)$). To create a normalizing flow model of sufficient capacity, many layers of bijective functions can be composed together:

$$z = f_\theta(x) = (f_1 \circ f_2 \circ \dots \circ f_i)(x), \quad (4)$$

$$x = g_\theta(z) = (f_i^{-1} \circ f_{i-1}^{-1} \circ \dots \circ f_1^{-1})(z), \quad (5)$$

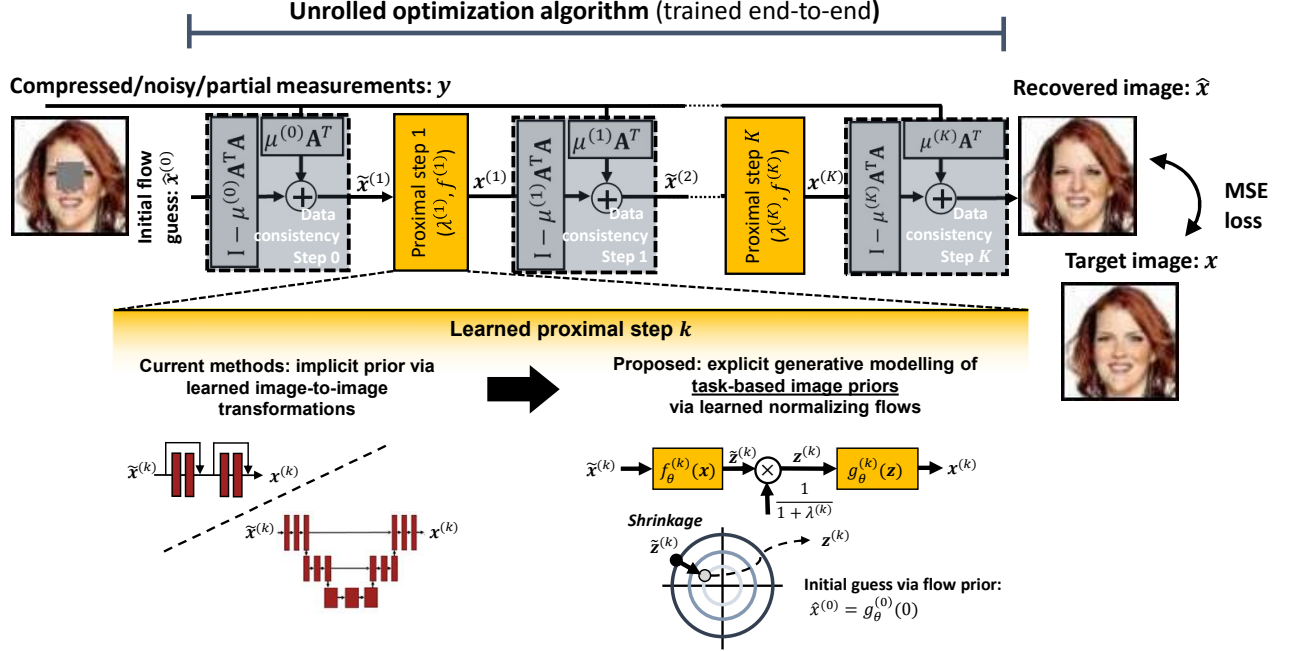


Fig. 1. Overview of the proposed algorithm. We unroll the iterations of a proximal gradient algorithm as a deep neural network. The proximal step performs shrinkage in the latent space of a normalizing flow prior, successively pushing the image likelihood in that distribution across the folds.

where ‘ \circ ’ denotes the composition of two functions, and θ are the parameters of the model. Details of the specific normalizing flow model we adopted, and its parameterization, are given in section V. Exact density evaluation of $p_\theta(x)$ is possible through the use of the change of variables formula, leading to:

$$\log p_\theta(x) = \log p(z) + \log |\det Df_\theta(x)|, \quad (6)$$

where D is the Jacobian, accounting for the change in density caused by the transformation f_θ .

With latent z following a (zero-mean, unity-variance) normal distribution and $x = g_\theta(z)$, we can rewrite (3) to perform the optimization in latent space:

$$\begin{aligned} \hat{z} &= \arg \min_z \frac{1}{2\sigma_n^2} \|y - \mathbf{A}g_\theta(z)\|_2^2 - \log p(z) \\ &= \arg \min_z \|y - \mathbf{A}g_\theta(z)\|_2^2 + \lambda \|z\|_2^2, \end{aligned} \quad (7)$$

where λ is a parameter that balances the importance of adhering to the measurements (data consistency) and the prior.

B. Unrolled proximal gradient iterations

The optimization problem in (7) can be solved using an iterative proximal-style algorithm that alternates between gradient updates in the direction of the data consistency term and pushing the solution in the proximity of the prior. We here unfold this iterative algorithm as a K -fold feedforward neural network that we train end-to-end.

To derive our iterative scheme, we will alternate using the problem formulations in (3) and (7). More specifically, at every

fold k the network performs data consistency updates using the x -space formulation in equation (3):

$$\tilde{x}^{(k+1)} = x^{(k)} - \mu^{(k)} A^T (y - Ax^{(k)}) \quad (8)$$

where superscript (k) denotes the current fold and $\mu^{(k)}$ is the trainable step size. The signal representation is then converted to the latent space:

$$\tilde{z}^{(k+1)} = f_\theta^{(k+1)}(\tilde{x}^{(k+1)}) \quad (9)$$

The purpose of this conversion to latent space is so that we may perform the proximal update $\mathcal{P}(\cdot)$ using the z -space formulation in (7):

$$z^{(k+1)} = \mathcal{P}^{(k+1)}(\tilde{z}^{(k+1)}) = \frac{\tilde{z}^{(k+1)}}{1 + \lambda^{(k+1)}} \quad (10)$$

where $\lambda^{(k+1)}$ is a trainable shrinkage parameter. Intuitively, this can be understood as pushing solutions into a high likelihood regime (i.e. closer to the origin in z). Finally, we convert from latent space back to signal space

$$x^{(k+1)} = g_\theta^{(k+1)}(z^{(k+1)}) \quad (11)$$

and continue on to the next iteration.

After K folds the final estimate \hat{x} is produced from the latent space after data consistency:

$$\hat{x} = g_\theta^{(K)}(\tilde{z}^{(K)}). \quad (12)$$

C. End-to-end task-adaptive training and initial guess

We make use of a pre-trained single generative normalizing flow model from a set of clean images to learn a generic density function (the experiment shows pre-training the normalizing

flow model leads to better results than not pre-training is in the Appendix). After pre-training, we embed these generic priors into the unrolled architecture and tailor it to the specific recovery task at hand using end-to-end supervised learning. This yields an architecture in which each fold has a distinct and task-based flow model.

Moreover, we make use of the explicit likelihood modeling of the normalizing flow prior to yield a useful initial guess for x : the maximum likelihood solution according to the clean images, by exploiting the fact that the most likely image lives at $z = 0$. This serves as an input to our network and is denoted by $\hat{x}^{(0)} = g_{\theta}^{(0)}(z^{(0)} = 0)$ - see also figure 1.

V. NORMALIZING FLOW ARCHITECTURE

For the normalizing flow model we make use of GLOW [32], a normalizing flow architecture that uses 1×1 convolutions to permute the dimensions on a multi-scale architecture [46]. Central to GLOW is the affine transformation, which is defined as:

$$y = s \cdot x + t, \quad (13)$$

where s is the scale, and t is the translation that is applied to x . In general, each step of GLOW consists of three stages: actnorm, an invertible 1×1 convolution, and an affine coupling layer. The actnorm stage (short for activation normalization) is a normalization scheme that is better adapted to low batch sizes than conventional batch normalization. The actnorm stage is implemented as an affine transformation that acts upon the incoming data, with learnable scale and translation parameters.

After normalization an invertible 1×1 convolution is performed. This convolution can be viewed as a generalization of a permutation operation. Permutation of the dimensions is a vital step in normalizing flow to ensure that each dimension can affect every other dimension, enabling the model to transform complex (data) distributions into normal distributions. By learning this permutation as a convolution, rather than choosing it *a-priori*, the permutation can more powerfully adapt to the data and/or task.

Lastly, each step of GLOW is concluded with an affine coupling layer. Where the scale and translation parameters are created from part of the incoming tensor, using:

$$\begin{aligned} x_a, x_b &= \text{split}(x) \\ (\log s, t) &= \text{NN}(x_b) \\ s &= \exp(\log s) \\ y_a &= s \cdot x_a + t y_b = x_b \\ y &= \text{concat}(y_a, y_b), \end{aligned}$$

where NN is a neural network that is not required to be invertible, as its input is known in both directions ($y_b = x_b$).

These steps are then combined within a multi-scale architecture [46] having 6 levels and a depth of 32. We refer the reader to [32] for further details regarding GLOW.

VI. EXPERIMENTS

We assess our method’s performance for various image recovery tasks on both the in-distribution images of human

faces, using the CelebA dataset, and the out-of-distribution images (see Appendix B). Across all experiments we used $K = 5$ folds of the unfolded proximal gradient algorithm.

A. Training strategy

The first step is to pre-train a Glow model. We leverage the existing pre-trained model from [6]. The pre-trained Glow architecture consists of a sequence of affine transformations with a depth of flow 18. The number of multi-scale levels is 4. A total of 23,000 training images from the CelebA-HQ dataset are used [47]. They are cropped to the faces, and resized to a size of 64×64 with 3 color channels. The model is trained on maximizing the data-likelihood given in by:

$$\log p(D|\theta) = \sum_{i=1}^N [\log p_z(f_{\theta}(x_i)) + \log |\det Df_{\theta}(x_i)|]. \quad (14)$$

After pre-training, We untie the weights of the Glow models at every fold. We then train the proximal gradient network making use of the CelebA Dataset [48], from which we exclude all images that are not of faces and then crop. This results in 10,000 images, in total of size 64×64 pixels, each with 3 color channels. We split the dataset into 992 training, 200 validation, and 200 testing images, and normalize them between -0.5 and 0.5. We train the proximal gradient network for the specific image recovery tasks using a Mean Square Error (MSE) loss. We again employ the Adam optimizer with ($\text{lr} = 1e^{-5}$, $\beta_1 = 0.9$, $\beta_2 = 0.999$, and $\epsilon = 1e - 8$). Moreover, we train the learnable step size $\mu^{(k)}$, and shrinkage factor $\lambda^{(k)}$ with a higher learning rate, namely $1e^{-2}$. As before, we perform early stopping based on the validation loss. Leveraging the invertible nature of the glow model, we strongly reduce train-time memory of the full unfolded architecture using the approach by Putzky and Welling [49]; instead of storing all intermediate activations for back-propagation, the proximal-gradient outputs after each fold are calculated on the fly.

B. Baselines

We compare our generative flow-based priors, with 25.78M parameters, to two alternative neural proximal mappings; one based on ResNets [9], with 0.16M parameters, and one based on a U-net with 31.04M parameters. Note that for fair and direct comparison, we focus on typical alternatives *within* the unfolded proximal gradient framework. This allows for straightforward assessment of the merit of the proposed (task-adapted) normalizing flow priors, beyond the architectural advantages of unfolding the proximal gradient algorithm itself. Training settings and strategy are identical to those described in section VI-A.

Our ResNet proximal baseline follows the structure proposed by Mardani *et al.*, [9]. Each residual block consists of two convolutional layers (3×3 kernel and 128 feature maps), followed by batch normalization and ReLU activation. This is then followed by another 3 convolutional layers with 1×1 kernels. Mardani *et al.* found that using 2 such residual blocks per proximal fold works best, so we follow that here as well. Our second baseline proximal mapping is a standard U-net

TABLE I
EXPERIMENTAL RESULTS OF DEEP UNFOLDING WITH NORMALIZING FLOW PRIORS COMPARED TO TWO STRONG BASELINES. VALUES REPORTED ARE MEAN PEAK SIGNAL TO NOISE RATIO (PSNR) OF THE RECONSTRUCTED IMAGES ACROSS THE TEST SET.

Experiment (settings)	ResNet Prox [9]	U-Net Prox [45]	Glow Prox (ours)
Denoising ($\eta \sim \mathcal{N}(\mu_n = 0, \sigma_n = 0.1)$)	27.957 dB	27.977 dB	29.062 dB
Denoising ($\eta \sim \mathcal{N}(\mu_n = 0, \sigma_n = 0.2)$)	26.559 dB	26.773 dB	27.566 dB
Inpainting ($W = 19 \times 19$)	32.504 dB	32.729 dB	34.720 dB
Deblurring ($\sigma_b = 5$)	32.340 dB	28.091 dB	33.301 dB

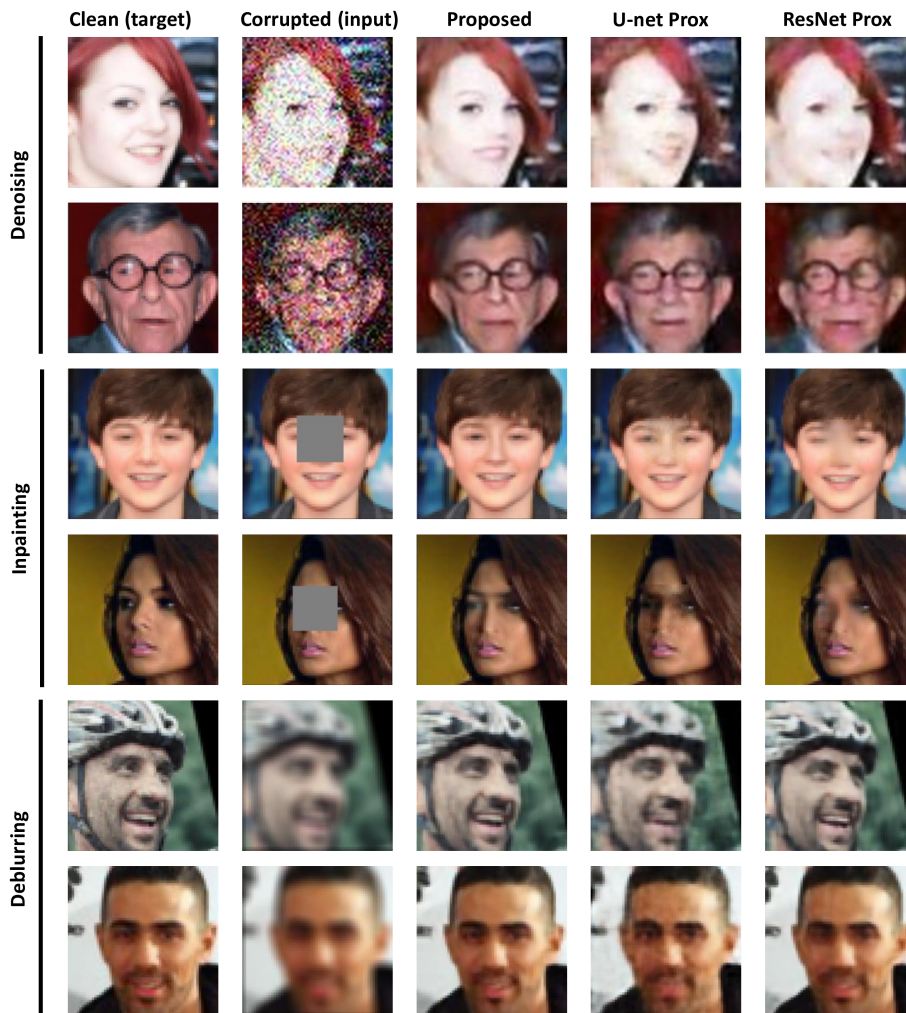


Fig. 2. Comparison of the proposed normalizing flows proximal mapping with baselines based on standard U-net or ResNet proximal mappings across the in-distribution dataset. Results are shown for 3 image restoration tasks applied to 6 typical example images.

[45] implementation. The U-net is a fully convolutional neural network that consists of a contracting path and an expansive path with skip connections between the two. This allows for learning both low-level and high-level features. We here make use of the Pytorch U-Net implementation.

C. Denoising

1) *Experiment setup:* We consider noisy measurements $y = x + \eta$, where η is an i.i.d. Gaussian noise vector with standard deviation σ_n and mean $\mu_n = 0$. Note that \mathbf{A} in (8) is thus an

identity matrix here. We analyze performance for two noise levels, $\sigma_n = 0.1$ and $\sigma_n = 0.2$. The goal of the recovery algorithm is to denoise the image, recovering x from y

2) *Results:* Table I shows that the proposed GLOW prox outperforms the baselines by about 1 dB PSNR for both noise levels. Qualitatively, this also becomes apparent from the examples displayed in figure 2 (top two rows). The challenging example in the second row shows how the most important features (note e.g. the cheeks) are better preserved using the GLOW prox.

D. Inpainting

1) *Experiment setup*: We perform measurements $y = Ax$, where A is a matrix masking the center $W = 19 \times 19$ elements of an image by operating on its vectorized form x . The goal of the recovery algorithm is to “inpaint” the masked pixels as accurately as possible.

2) *Results*: For inpainting, the performance gain using GLOW is about 2dB (see table I). Visual inspection of the first inpainting example given in row 3 of figure 2 shows that the proposed method is better capable of producing high-resolution reconstructions. Note that this apparent higher fidelity is paired with a pixel-wise PSNR improvement: reconstructions are not merely visually pleasing, but also more accurate. We again also include a highly challenging example (row 4): while all methods fail to reconstruct the actual shape of the nose, the proposed method does produce improved skin tone compared to the surroundings of the inpainted area.

E. Deblurring

1) *Experiment setup*: We take measurements $y = Ax$, where A is a 2D convolution matrix blurring the image with a Gaussian kernel having standard deviation $\sigma_b = 5$ pixels. We analyze the performance of our method in recovering the original image from the blurred measurements, i.e. deblurring.

2) *Results*: As for the other tasks, the proposed GLOW prox outperforms the other baselines (see table I). While the performance gain is about 1dB PSNR with respect to the ResNet prox, the U-Net prox performs significantly worse for this particular experiment. Figure 2 shows two illustrative examples from which this difference is apparent. While the qualitative improvement of GLOW- over ResNet-based proximal mappings is less striking, one can e.g. notice it from the details around the eyes and cheeks.

VII. CONCLUSION

In this paper we proposed a framework for deep algorithm unfolding based on task-adapted normalizing flow priors. Our method first learns generic priors on a given train dataset, and then adapts these to the specific image restoration task at hand. We evaluated the performance of our approach for a variety of such tasks, i.e., image denoising, inpainting and deblurring, and demonstrate performance gains compared to strong baselines. Beyond image restoration, we expect our method to find applications in compressed sensing and medical image reconstruction, which is part of future work.

APPENDIX A

INITIAL GUESS: MAXIMUM LIKELIHOOD PRIOR

We make use of the explicit likelihood modeling of our normalizing flow prior to yield a useful initial guess: the maximum likelihood solution according to the distribution of clean images. This image is visualized in figure 3.

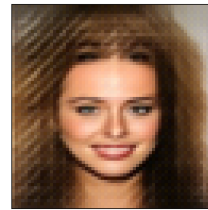


Fig. 3. Visualization of our initial guess: the maximum likelihood image according to the flow prior.

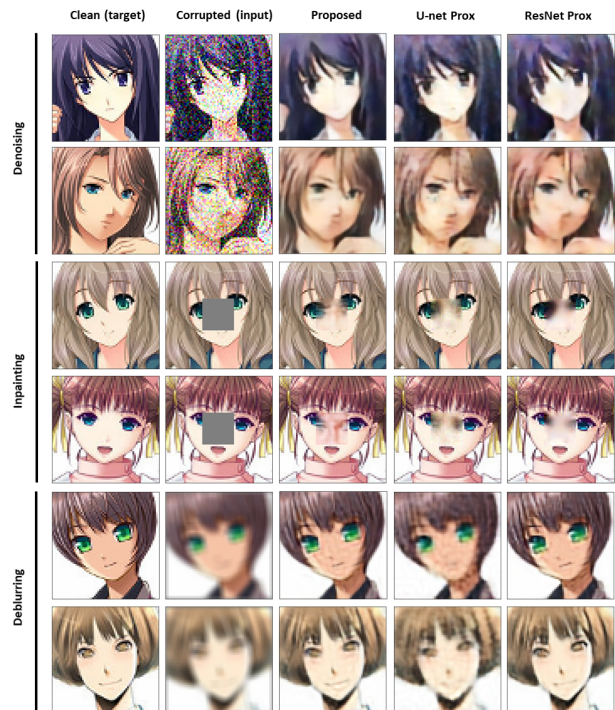


Fig. 4. Comparison of the proposed normalizing flows proximal mapping with baselines based on standard U-net or ResNet proximal mappings. Results are shown for the denoising, inpainting and deblurring tasks applied to 6 typical out-of-distribution images.

APPENDIX B

MORE EXPERIMENTS ON OUT-OF-DISTRIBUTION DATASET

We also evaluate the behaviour of the proposed method on out-of-distribution data. To that end, we tested our models trained on the CelebA dataset on images from the Anime Faces set. The original images were taken from here. As a preprocessing step, the faces are detected and cropped to sizes 64×64 (details can be found on github). The images in this out-of-distribution set show clear differences with respect to the train set, such as much bigger eyes and much smaller noses. We evaluate performance on 100 images that were randomly selected from the full dataset.

While performance deteriorates for out of distribution prediction, our proposed model still outperforms our two baselines, gaining 0.1 dB, 0.1dB, 0.4dB in the image denoising, inpainting and deblurring tasks, respectively, see table II. Example images for visual assessment are given in Fig. 4. Interestingly, visual comparison qualitatively shows a stronger “CelebA” image prior in the reconstructions by the proposed

model compared to the ResNet-based reconstructions. This is particularly evident from the inpainting task, where natural noses and eyes are painted into the unnatural Anime faces. In this case the ResNet-based reconstructions are more smooth and blurry, with a less clear “CelebA fingerprint”.

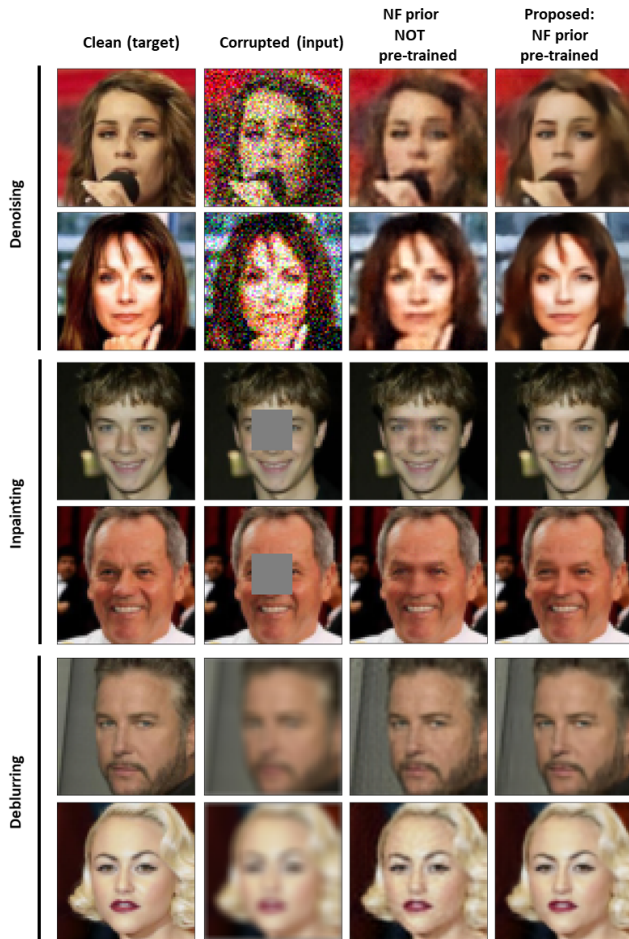


Fig. 5. Comparison of the normalizing flows proximal mapping with pre-training (proposed) and without pre-training. Results are shown for 3 image restoration tasks applied to 6 typical example images.

APPENDIX C

PRE-TRAINING NORMALIZING FLOW (NF) PRIOR

We investigated whether pre-training a NF prior and subsequently fine-tuning its instances within the unfolded scheme achieves better results than training the flow models directly from scratch. To this end, we used the same training setup as detailed in the main body of the paper and test it on the test set of the CelebA [48] dataset. For the denoising, inpainting and deblurring tasks, the performance gains using a pre-trained NF prior are 1 dB, 1.8 dB and 0.6 dB, respectively (see table III). A series of illustrative example images, comparing both training strategies, are shown in Fig. 5.

REFERENCES

- [1] N. Pezzotti, S. Yousefi, M. S. Elmahdy, J. Van Gemert, C. Schülke, M. Doneva, T. Nielsen, S. Kastrulyin, B. P. Lelieveldt, M. J. Van Osch *et al.*, “An adaptive intelligence algorithm for undersampled knee mri reconstruction: Application to the 2019 fastmri challenge,” *arXiv preprint arXiv:2004.07339*, 2020.
- [2] F. D. M. Neto and A. J. da Silva Neto, *An introduction to inverse problems with applications*. Springer Science & Business Media, 2012.
- [3] D. L. Donoho, “Compressed sensing,” *IEEE Transactions on information theory*, vol. 52, no. 4, pp. 1289–1306, 2006.
- [4] Y. C. Eldar and G. Kutyniok, *Compressed sensing: theory and applications*. Cambridge university press, 2012.
- [5] M. Asim, F. Shamshad, and A. Ahmed, “Blind image deconvolution using deep generative priors,” *IEEE Transactions on Computational Imaging*, vol. 6, pp. 1493–1506, 2020.
- [6] M. Asim, M. Daniels, O. Leong, P. Hand, and A. Ahmed, “Invertible generative models for inverse problems: mitigating representation error and dataset bias,” in *Proceedings of Machine Learning and Systems 2020*, 2020, pp. 4577–4587.
- [7] V. Monga, Y. Li, and Y. C. Eldar, “Algorithm unrolling: Interpretable, efficient deep learning for signal and image processing,” *arXiv preprint arXiv:1912.10557*, 2019.
- [8] K. Gregor and Y. LeCun, “Learning fast approximations of sparse coding,” ser. ICML’10, 2010, p. 399–406.
- [9] M. Mardani, Q. Sun, S. Vasawanala, V. Pappas, H. Monajemi, J. M. Pauly, and D. L. Donoho, “Neural proximal gradient descent for compressive imaging,” *CoRR*, vol. abs/1806.03963, 2018.
- [10] Y. LeCun, Y. Bengio, and G. Hinton, “Deep learning,” *Nature*, vol. 521, no. 7553, pp. 436–444, May 2015.
- [11] H. Burger, C. Schuler, and S. Harmeling, “Image denoising: Can plain neural networks compete with bm3d?” 06 2012, pp. 2392–2399.
- [12] C. Tian, L. Fei, W. Zheng, Y. xu, W. Zuo, and C.-W. Lin, “Deep learning on image denoising: An overview,” *Neural Networks*, vol. 131, 08 2020.
- [13] H. Burger, C. Schuler, and S. Harmeling, “Image denoising: Can plain neural networks compete with bm3d?” *2012 IEEE Conference on Computer Vision and Pattern Recognition*, pp. 2392–2399, 2012.
- [14] P. Vincent, H. Larochelle, Y. Bengio, and P.-A. Manzagol, “Extracting and composing robust features with denoising autoencoders,” 01 2008, pp. 1096–1103.
- [15] J. Xie, L. Xu, and E. Chen, “Image denoising and inpainting with deep neural networks,” in *Proceedings of the 25th International Conference on Neural Information Processing Systems - Volume 1*, ser. NIPS’12. Red Hook, NY, USA: Curran Associates Inc., 2012, p. 341–349.
- [16] L. Xu, J. S. J. Ren, C. Liu, and J. Jia, “Deep convolutional neural network for image deconvolution,” in *Proceedings of the 27th International Conference on Neural Information Processing Systems - Volume 1*, ser. NIPS’14. Cambridge, MA, USA: MIT Press, 2014, p. 1790–1798.
- [17] U. Demir and G. B. Ünal, “Patch-based image inpainting with generative adversarial networks,” *CoRR*, vol. abs/1803.07422, 2018.
- [18] K. Nazeri, E. Ng, T. Joseph, F. Z. Qureshi, and M. Ebrahimi, “Edgeconnect: Generative image inpainting with adversarial edge learning,” *CoRR*, vol. abs/1901.00212, 2019.
- [19] K. Kulkarni, S. Lohit, P. Turaga, R. Kerviche, and A. Ashok, “Reconnet: Non-iterative reconstruction of images from compressively sensed measurements,” in *2016 IEEE Conference on Computer Vision and Pattern Recognition (CVPR)*, 2016, pp. 449–458.
- [20] D. M. Pelt and K. J. Batenburg, “Fast tomographic reconstruction from limited data using artificial neural networks,” *IEEE Transactions on Image Processing*, vol. 22, no. 12, pp. 5238–5251, 2013.
- [21] D. Boubilil, M. Elad, J. Shtok, and M. Zibulevsky, “Spatially-adaptive reconstruction in computed tomography using neural networks,” *IEEE Transactions on Medical Imaging*, vol. 34, no. 7, pp. 1474–1485, 2015.
- [22] K. H. Jin, M. T. McCann, E. Froustey, and M. Unser, “Deep convolutional neural network for inverse problems in imaging,” *IEEE Transactions on Image Processing*, vol. 26, no. 9, pp. 4509–4522, 2017.
- [23] Y. Fang, L. Liu, P. Haipeng, J. Kurths, and Y. Yang, “Overview of compressed sensing: Sensing model, reconstruction algorithm, and its applications,” *Applied Sciences*, vol. 10, p. 5909, 08 2020.
- [24] A. Bora, A. Jalal, E. Price, and A. G. Dimakis, “Compressed sensing using generative models,” 2017.
- [25] S. Boyd, N. Parikh, E. Chu, B. Peleato, and J. Eckstein, “Distributed optimization and statistical learning via the alternating direction method of multipliers,” *Foundations and Trends in Machine Learning*, vol. 3, no. 1, pp. 1–122, 2011.
- [26] R. Deriche, P. Kornprobst, and M. Nikolova, “Half-quadratic regularization for mri image restoration,” 05 2003, pp. VI – 585.

TABLE II

EXPERIMENTAL RESULTS OF DEEP UNFOLDING WITH NORMALIZING FLOW PRIORS COMPARED TO TWO BASELINES. VALUES REPORTED ARE MEAN PEAK SIGNAL TO NOISE RATIO (PSNR) OF THE RECONSTRUCTED IMAGES ACROSS THE OUT-OF-DISTRIBUTION TEST SET.

Experiment (settings)	ResNet Prox [9]	U-Net Prox [45]	Glow Prox (ours)
Denoising $\eta \sim \mathcal{N}(\mu_n = 0, \sigma_n = 0.1)$	21.878 dB	21.295 dB	22.006 dB
Denoising $\eta \sim \mathcal{N}(\mu_n = 0, \sigma_n = 0.2)$	21.293 dB	21.023 dB	21.396 dB
Inpainting $W = 19 \times 19$	23.704 dB	23.837 dB	24.047 dB
Deblurring $\sigma_b = 5$	22.896 dB	20.191 dB	23.382 dB

TABLE III

EXPERIMENTAL RESULTS OF DEEP UNFOLDING WITH NORMALIZING FLOW PRIORS COMPARED BETWEEN WITH PRE-TRAINING(PROPOSED) AND WITHOUT PRE-TRAINING. VALUES REPORTED ARE MEAN PEAK SIGNAL TO NOISE RATIO (PSNR) OF THE RECONSTRUCTED IMAGES ACROSS THE IN-DISTRIBUTION TEST SET.

Experiment (settings)	Glow Prox Without pre-training	Glow Prox (Ours) With pre-training
Denoising $\eta \sim \mathcal{N}(\mu_n = 0, \sigma_n = 0.1)$	27.918 dB	29.062 dB
Denoising $\eta \sim \mathcal{N}(\mu_n = 0, \sigma_n = 0.2)$	26.373 dB	27.566 dB
Inpainting $W = 19 \times 19$	32.928 dB	34.720 dB
Deblurring $\sigma_b = 5$	32.647 dB	33.301 dB

- [27] O. Ronneberger, P. Fischer, and T. Brox, "U-net: Convolutional networks for biomedical image segmentation," in *Medical Image Computing and Computer-Assisted Intervention (MICCAI)*, ser. LNCS, vol. 9351. Springer, 2015, pp. 234–241.
- [28] K. He, X. Zhang, S. Ren, and J. Sun, "Deep residual learning for image recognition," in *2016 IEEE Conference on Computer Vision and Pattern Recognition (CVPR)*, 2016, pp. 770–778.
- [29] K. Zhang, Y. Li, W. Zuo, L. Zhang, L. V. Gool, and R. Timofte, "Plug-and-play image restoration with deep denoiser prior," 2020.
- [30] I. Goodfellow, J. Pouget-Abadie, M. Mirza, B. Xu, D. Warde-Farley, S. Ozair, A. Courville, and Y. Bengio, "Generative adversarial nets," in *Advances in Neural Information Processing Systems*, Z. Ghahramani, M. Welling, C. Cortes, N. Lawrence, and K. Q. Weinberger, Eds. Curran Associates, Inc., pp. 2672–2680.
- [31] D. P. Kingma and M. Welling, "Auto-encoding variational bayes," 2014.
- [32] D. P. Kingma and P. Dhariwal, "Glow: Generative flow with invertible 1x1 convolutions," *arXiv preprint arXiv:1807.03039*, 2018.
- [33] P. Hand, O. Leong, and V. Voroninski, "Phase retrieval under a generative prior," in *Proceedings of the 32nd International Conference on Neural Information Processing Systems*, ser. NIPS'18. Red Hook, NY, USA: Curran Associates Inc., 2018, p. 9154–9164.
- [34] P. Hand and V. Voroninski, "Global guarantees for enforcing deep generative priors by empirical risk," *IEEE Transactions on Information Theory*, vol. 66, no. 1, pp. 401–418, 2020.
- [35] M. Asim, F. Shamshad, and A. Ahmed, "Solving bilinear inverse problems using deep generative priors," *CoRR*, vol. abs/1802.04073, 2018.
- [36] J. Hershey, J. Le Roux, and F. Weninger, "Deep unfolding: Model-based inspiration of novel deep architectures," 09 2014.
- [37] y. Yang, J. Sun, H. Li, and Z. Xu, "Deep admm-net for compressive sensing mri," in *Advances in Neural Information Processing Systems*, vol. 29. Curran Associates, Inc., 2016, pp. 10–18.
- [38] J. Zhang and B. Ghanem, "Ista-net: Interpretable optimization-inspired deep network for image compressive sensing," in *2018 IEEE/CVF Conference on Computer Vision and Pattern Recognition*, 2018, pp. 1828–1837.
- [39] C. A. Metzler, A. Maleki, and R. G. Baraniuk, "From denoising to compressed sensing," *IEEE Transactions on Information Theory*, vol. 62, no. 9, pp. 5117–5144, 2016.
- [40] C. A. Metzler, A. Mousavi, and R. G. Baraniuk, "Learned d-amp: Principled neural network based compressive image recovery," 2017.
- [41] S. Wang, S. Fidler, and R. Urtasun, "Proximal deep structured models," in *Advances in Neural Information Processing Systems*, vol. 29. Curran Associates, Inc., 2016, pp. 865–873.
- [42] J. Adler and O. Oktem, "Learned primal-dual reconstruction," *IEEE Transactions on Medical Imaging*, vol. 37, no. 6, p. 1322–1332, Jun 2018.
- [43] W. Dong, P. Wang, W. Yin, G. Shi, F. Wu, and X. Lu, "Denoising prior driven deep neural network for image restoration," *CoRR*, vol. abs/1801.06756, 2018.
- [44] K. Zhang and R. Timofte, "Deep unfolding network for image super-resolution," 06 2020, pp. 3214–3223.
- [45] O. Ronneberger, P. Fischer, and T. Brox, "U-net: Convolutional networks for biomedical image segmentation," in *International Conference on Medical image computing and computer-assisted intervention*. Springer, 2015, pp. 234–241.
- [46] S. B. Laurent Dinh, Jascha Sohl-Dickstein, "Density estimation using real nvp," 5 2016.
- [47] S. L. J. L. Tero Karras, Timo Aila, "Progressive growing of gans for improved quality, stability, and variation," in *The International Conference on Learning Representations (Virtual) (ICLR)*, Feb 2018.
- [48] Z. Liu, P. Luo, X. Wang, and X. Tang, "Deep learning face attributes in the wild," in *Proceedings of International Conference on Computer Vision (ICCV)*, December 2015.
- [49] P. Putzky and M. Welling, "Invert to learn to invert," in *Advances in Neural Information Processing Systems 32*, H. Wallach, H. Larochelle, A. Beygelzimer, F. d'Alché-Buc, E. Fox, and R. Garnett, Eds. Curran Associates, Inc., 2019, pp. 444–454.